Convective Inhibition as a Predictor of Convection during AVE-SESAME II

FRANK P. COLBY, JR.[1]

Department of Meteorology and Physical Oceanography, Massachusetts Institute of Technology, Cambridge, MA 02139

(Manuscript received 1 July 1983, in final form 21 August 1984)

ABSTRACT

The AVE-SESAME II data set of 19 April 1979 is examined to determine the thermodynamic conditions prior to the onset of deep convection in western Kansas. The observations indicate that the convective region was characterized locally by substantial potential convective energy and low convective inhibition above the boundary layer.

One-dimensional modeling shows that the convection occurred where the convective inhibition was a minimum, but not where the potential convective energy was a maximum. The model results suggest that the convective inhibition above the boundary layer was almost zero when the first echoes were observed.

1. Introduction

Prior to deep afternoon convection in the central United States in springtime, the environment is usually characterized by an atmospheric boundary layer (ABL) which is thermodynamically well-mixed and capped by a stable layer. The ABL is assumed in this paper to be that layer in the atmosphere not touching the ground, but, nevertheless, largely dominated by surface-based fluxes. This definition presumes the existence of a relatively thin surface layer between the ABL and the ground. Deep convection requires the presence of a conditionally unstable lapse rate, so that parcels lifted adiabatically from the ABL become more buoyant than their environment. The latent heat released by condensation provides the thermal energy required to give positive buoyancy. Since ABL parcels cannot rise spontaneously through the stable layer capping the ABL, deep convection usually requires a lifting mechanism to provide vertical momentum sufficient to carry parcels from the ABL to their level of free convection. The research reported in this paper indicates that the immediate region containing the convective outbreak was characterized by a minimum in stability above the ABL.

Lifting mechanisms have been discussed extensively in the recent literature. Gravity waves have been implicated by many investigators, including Uccellini (1975) and Miller and Sanders (1980). Sun and Ogura (1979) and Cooper *et al.* (1982) considered sea-breeze type circulations as possible mechanisms. Outflow from mature storms can initiate new convection as shown by Maddox *et al.* (1980) and Matthews (1981). Holle and Maier (1980) implied that this type of lifting mechanism was also responsible for a tornadic storm in Florida. Frontal circulations have also been held responsible for deep convection, such as in Sanders and Paine (1975). Uccellini and Johnson (1979) suggested jet streak circulations as lifting mechanisms.

Beebe (1958) and others examined the thermal structure of the vicinity of convection. Beebe showed that the stable layer above the boundary layer was usually eroded prior to tornado outbreaks, and, in some cases, the stable layer disappeared entirely. Some early work was aimed at forecasting convection on the basis of vertical thermodynamic structure; thus, operational forecasters have the Showalter index (Showalter, 1953) and the Lifted index (Galway, 1956) available today. Carlson *et al.* (1980) continued this type of research with development of a Lid Strength index.

One difficulty with the thermal structure in convective situations is that convection often occurs between available radiosonde observations, either in time or space. Spatial interpolation of soundings can be helpful to infer structure, but one is never sure whether the interpolation is valid for small-scale phenomena such as convection.

Many investigators have examined one case of deep afternoon convection from the archives of the National Severe Storms Laboratory in Norman, Oklahoma. The case of 8 June 1966 involved a squall line that formed in the afternoon on the western edge of the Laboratory's mesonetwork. Colby (1980) showed that a thermodynamically well-mixed ABL existed in a wide region containing the convective outreak region. His work revealed a gradient in mixed layer depth in the region, with deep dry ABLs to the

[1] Present affiliation: Department of Earth Sciences, University of Lowell, Lowell, MA 01854.

west and shallower more moist ABLs east of the outbreak area.

Interpolation of radiosonde data inferred the existence of a minimum in stability above the ABL in the area where the convection began. Sun and Ogura (1979) suggested that the lifting mechanism was due to an "inland sea breeze", which enhanced the mixed-layer height gradient. The convection began where the destabilization above the ABL was sufficient to allow ABL parcels to rise to their level of free convection (LFC). In this case, the primary factors were boundary layer heating and the associated inland sea-breeze circulation.

One can imagine a spectrum of combinations of heating and lifting mechanisms, depending upon specific situations. A frontal circulation would likely have strong vertical velocity and therefore require less destabilization from heating. On the other hand, dry line convection can take place in the presence of strong heating and a weak dynamic lifting mechanism.

This paper examines one data set from the Severe Environmental Storms and Mesoscale Experiment (SESAME). In this case of 19 April 1979, a squall line developed in a region of weak convergence. Analysis of data is as follows: plotting of hourly observations over a mesoscale region containing the outbreak area, examination of available radiosonde data for structure, computation of potential convective energy and convective inhibition and, finally, employment of a one-dimensional thermodynamic ABL model to determine the role of heating in the destabilization process which led to convection.

2. Definitions

The ABL is assumed to be well mixed above the surface layer, having constant potential temperature (Θ) and constant water vapor mixing ratio (q). A mean ABL parcel can then be defined by the values of Θ and q that characterize the well-mixed ABL. Averaging is required from observational soundings, since q sometimes decreases with height in an otherwise well-mixed ABL, as shown by Mahrt (1976) for Colorado soundings. Schaefer (1976) found that most of the "well-mixed" soundings he studied in Oklahoma have constant mixing ratio in the lower 90% of the layer, and a small decrease above that up to the mixed layer top.

Potential convective energy is measured by the ABL lifted index (L), as defined below. The mean ABL parcel rises dry-adiabatically until saturation, and pseudoadiabatically thereafter to 500 mb:

$$L = (\text{parcel's lifted 500 mb } T) - (\text{ambient 500 mb } T). \quad (1)$$

When lifted, unstable air will be warmer than the ambient atmosphere. Thus, a positive lifted index indicates unstable parcels, like the Lid Strength index (Carlson *et al.*, 1980) and unlike the operational Lifted index (Galway, 1956).

Convection inhibition (I) equals the negative work done by the mean ABL parcel as it rises through the stable layer to its level of free convection. Thus,

$$I = g \int \frac{T(\text{air}) - T(\text{parcel})}{TB}\, dz, \quad (2)$$

where TB is an average temperature for the layer. This represents an energy well that must be surpassed by the parcel to realize its potential convective energy. For an ABL parcel to rise through this stable layer, it must possess sufficient kinetic energy per unit mass, or an impulsive upward velocity w, such that

$$w = (2I)^{1/2} \quad (3)$$

(Petterssen, 1956).

3. Case study—19 April 1979

Weak synoptic-scale thermodynamic changes characterized the period 1100–2000 GMT, 19 April. Figure 1 shows the analyses of 500 mb height and temperature change during this period. A cold trough is located to the northwest in Wyoming, but Kansas experienced very small changes during this period.

The convection began along a line in western Kansas, between 2100 and 2200 GMT. A warm tongue appears on the 1200 GMT surface analysis (Fig. 2) as a large area of 298 to 300 K potential temperature in western Kansas and the Texas Panhandle. This tongue of warm air became warmer and more clearly defined during the day. By 1600 GMT (Fig. 3), the cool outflow from the active convection in the Panhandle distorted the shape of the tongue. To the north in western Kansas, skies remained mostly clear [cloud cover at Garden City, Kansas (GCK) and Goodland, Kansas (GLD) was cirrus], and the boundary layer heating continued. By 2100 GMT (not shown) a strong temperature gradient existed on the eastern edge of an intense warm tongue, and weak convergence developed in the surface winds across this gradient. By 2200 GMT (Fig. 4) convection erupted in western Kansas, but notice that the outbreak occurred on the warm side of the gradient near the axis of the warm tongue, in agreement with the findings of Darkow *et al.* (1958).

The boundary layer in the SESAME region developed in three modes during the day on 19 April 1979. In the first mode, as typified by the changes at GLD, a very deep and dry boundary layer evolved. Figure 5 shows the 1100 and 2000 GMT soundings at GLD. By 2000 GMT, the very dry boundary layer reached to nearly 600 mb.

A sounding at Dodge City, Kansas, (DDC) illustrates the second mode. Here, the boundary layer remained shallower and most moist. Notice in Fig. 6 that by 1700 GMT the well-mixed layer extended to

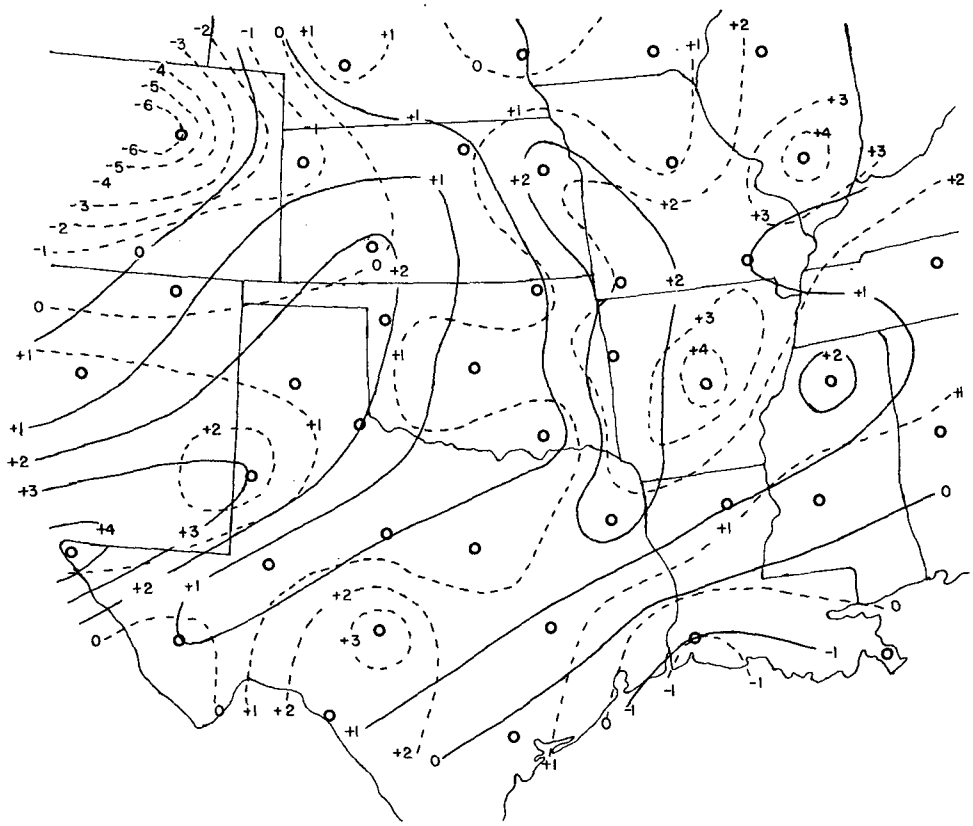

FIG. 1. Change of 500 mb temperature (°C) and height (dm) of 500 mb pressure surface from 1100 to 2000 GMT on 19 April 1979. Dashed lines are for temperature change and solid lines are for height change.

only 825 mb. By 2000 GMT (not shown) it still failed to reach 800 mb.

Both advection and surface heating produced these two modes of development. At DDC, moisture advection was negligible during the period 1100–2000 GMT. Goodland experienced dry advection from the west around 1600 GMT, but not enough to explain all of the remarkable drying of the GLD boundary layer.

Figure 7 shows the analysis of rainfall data for the previous calendar day, taken from Climatological Data for Kansas. Without any observations of soil surface moisture, this rainfall gives a rough approximation of the soil surface wetness. Although actual soil surface wetness is a function of soil type, runoff patterns, etc., this complex treatment was not performed for these data. A band of relatively wet soil lay along the region between DDC and Hill City, Kansas (HLC), while the area near GLD was dry.

With dry soil and high ground temperatures, the release of sensible heat from the ground probably dominated the energy balance near GLD. Near DDC, however, the evaporation of moisture from the soil probably used a significant portion of the incident radiation, leaving less energy for soil heating or sensible heat flux.

The greater sensible heat flux at GLD explains why the ABL grew deeper there than at DDC. The weaker moisture flux at GLD, plus greater ABL entrainment of dry air from aloft were the primary factors that made GLD's ABL so much drier. The advection made a relatively small contribution at GLD.

Other factors certainly had an influence on the pattern of ABL change as well. Since the initial depth of the layer below the inversion was much smaller in western Kansas than in eastern Kansas, the ABL needed less heating to reach its convective temperature. However, the shallowest initial depths were not found in the outbreak region.

An example of the third mode of ABL development is shown by the sounding at Concordia, Kansas (CNK) in Fig. 8. Here, drizzle early in the day and clouds throughout the day sharply curtailed heating. As a result, only a very shallow mixed layer developed.

Figure 9 shows the field of change of surface potential temperature and dew point for the period 1200–2200 GMT. To the west, where large increases

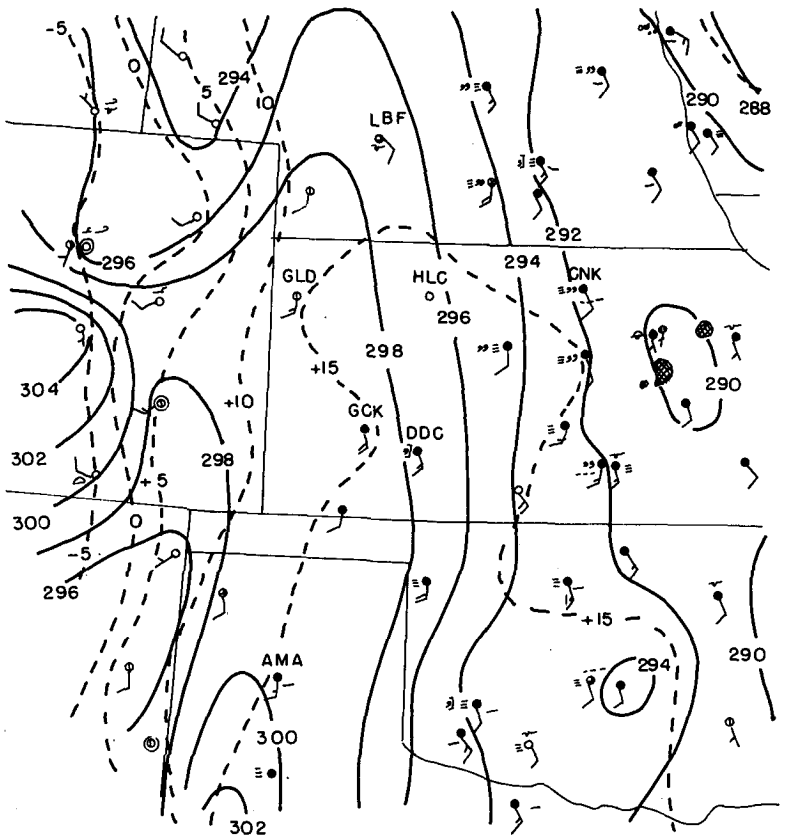

FIG. 2. Mesoscale surface analysis for 1200 GMT 19 April 1979. Solid lines are for surface potential temperature (K) and dashed lines are for dew point (°C). Winds (kt), sky conditions, cloud type and current weather (if reported) are plotted according to conventional synoptic code. Radar echoes of at least 20 dBz are denoted by the cross-hatched, irregularly shaped areas.

in potential temperature occurred, the ABL dried out too much for convection to occur. To the east, near CNK, cloud cover reduced the heating, although the ABL stayed moist. Strong heating (not the strongest) and a moderate drop in dew point characterized the area of outbreak. Calculations (shown in Table 1) made from analyses of surface hourly data at each end of the outbreak area demonstrate that the convective region experienced very little temperature advection. Advection contributed between 0 and 2 K to the change in potential temperature of 11 K.

Figure 10 shows the analysis of convective energy and inhibition calculated from the available 2000 GMT soundings. The radar echoes formed after 2000 GMT in a region of substantial convective energy rather than in the region of maximum convective energy. The echoes formed in a broad area of minimum inhibition. To obtain more detailed information on a smaller scale, a model was employed to simulate the thermodynamic changes in the ABL in the convective region.

4. Model

The model assumes the ABL to be well-mixed in heat and moisture. A surface layer of 5 mb depth exists between the ground and the ABL. This is an *ad hoc* representation of the real structure. The boundary layer changes occur due to the surface fluxes of latent and sensible heat. These fluxes are computed using boundary layer similarity theory, so the actual height of the interface between the surface layer and the ABL no longer appears explicitly in the equations. Therefore, the assumption of a constant pressure depth surface layer does not crucially affect the lifted index or convective inhibition of the atmosphere. Mahrt's (1976) data indicates that the surface layer depth is about 10% of the mixed layer depth, or between 0 and 10 mb for typical mixed layers.

The ABL above the surface layer is defined in the model by its potential temperature, its mixing ratio and its height. An inversion that has a strength and a depth caps the ABL. The input sounding gives the initial inversion depth. The top of the inversion remains constant until the ABL grows enough to absorb all of the inversion layer. The bottom of the inversion rises as the ABL grows by entraining air from the inversion layer into the ABL. The structure above the ABL comes directly from the data in the

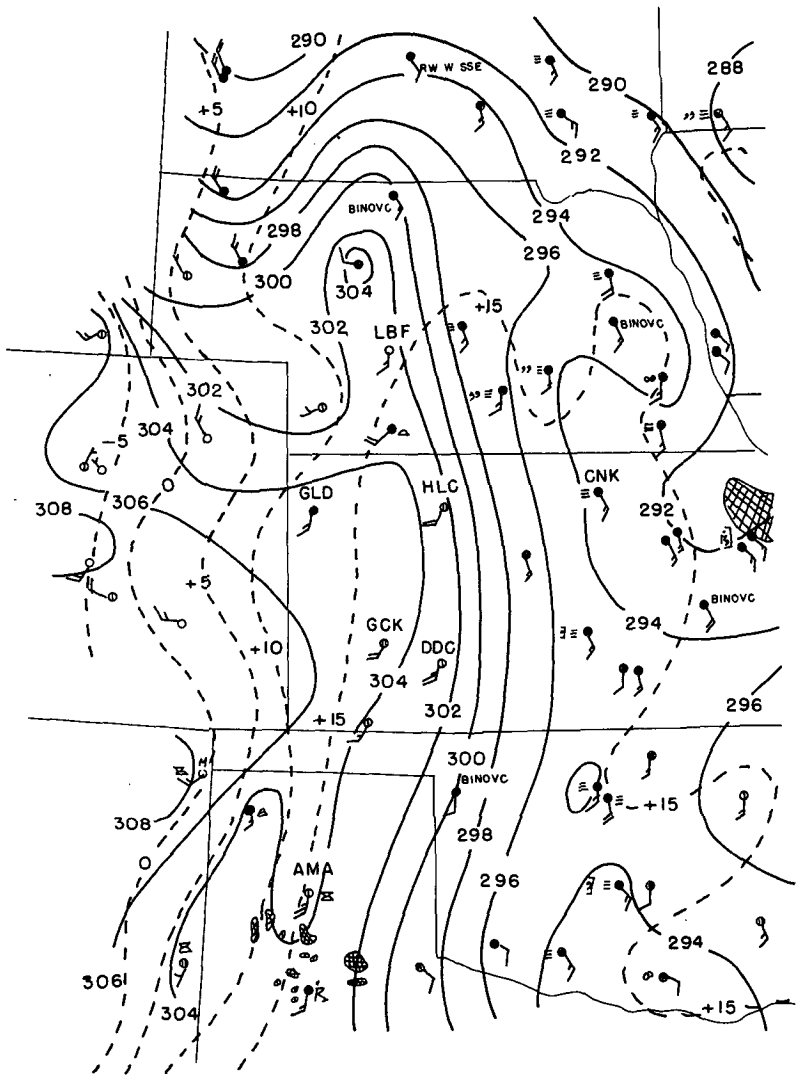

FIG. 3. As in Fig. 2 but for 1600 GMT.

original sounding. Figure 11 illustrates the assumed structure.

The model includes radiation, a surface energy balance and entrainment of the inversion by the turbulent ABL. The radiation parameterization, a routine originally designed for use in the UCLA General Circulation Model, follows Katayama (1972). The incident radiation and IR emission are calculated separately. The net flux divergence produces a mean temperature change for each model layer. The model assumes that specific humidity varies linearly with $\ln(p)$, which allows a simple integration of water content. The model includes a fixed amount of CO_2 based on experimental data, and so fixes its contribution for each layer. The radiation routines include clouds in a simple way. The effect varies linearly with the fractional cloud cover, and the IR calculation depends upon the thickness of the cloud layer. Clouds reflect some incident radiation, and the radiation that penetrates emerges as diffuse.

The surface energy balance is

$$NR = SH + LH + GS, \tag{4}$$

where NR is the net radiation incident on the surface, SH is the sensible heat flux upward from the surface, LH is the latent heat flux upward from the surface, and GS is the soil heat flux downward into the ground which heats the soil. Figure 11 illustrates the various fluxes and their directions.

Monin-Obukhov similarity theory for the ABL provides the basis for the parameterization of the sensible and latent heat fluxes. The fluxes depend upon the gradients in the surface layer, the depth of the boundary layer and the incident radiation. The theory assumes that the vertical structure of temper-

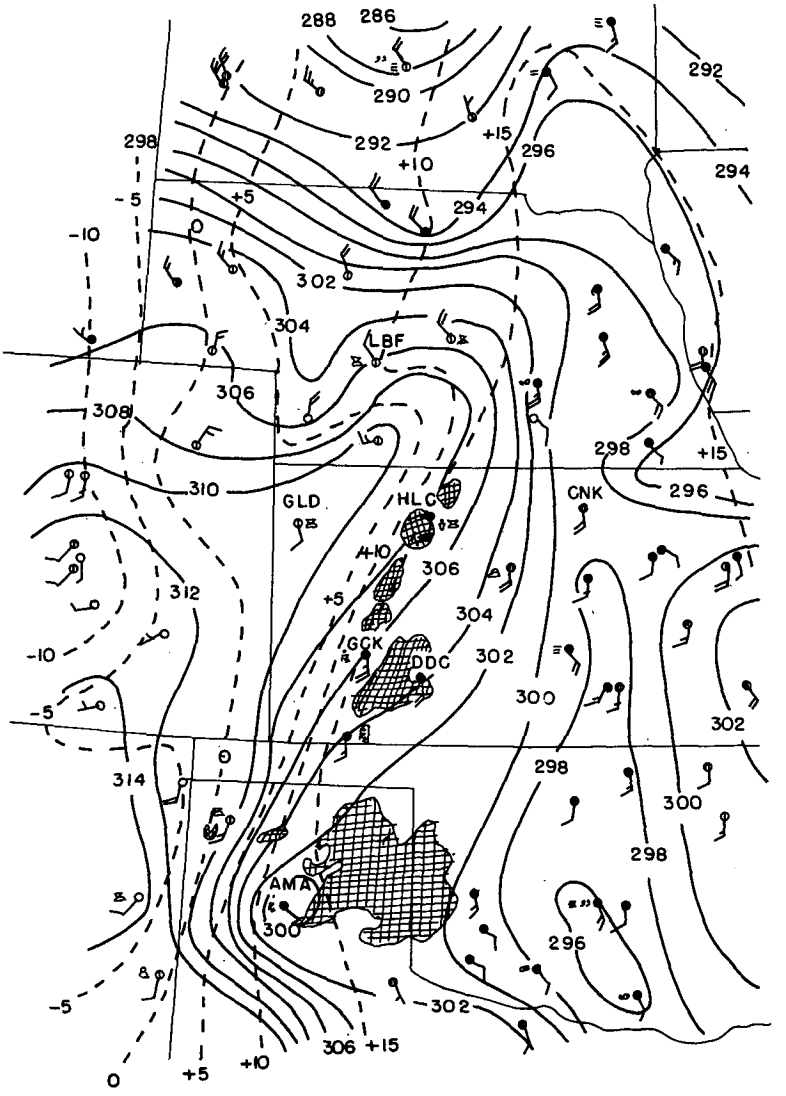

FIG. 4. As in Fig. 2 but for 2200 GMT.

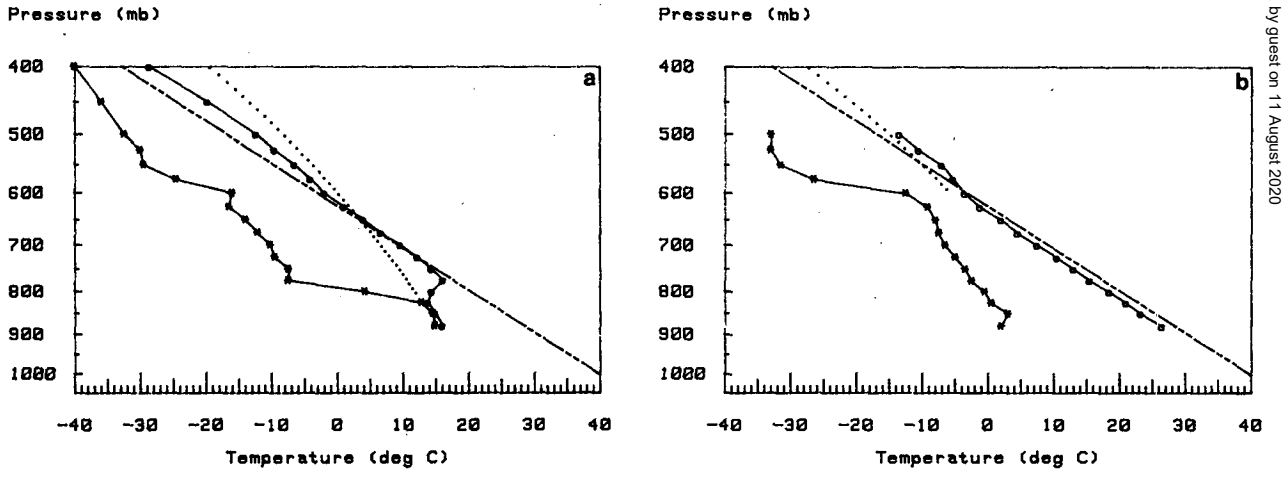

FIG. 5. Soundings plotted on a pseudoadiabatic diagram, from Goodland, Kansas for (a) 1124 GMT and (b) 2007 GMT 19 April 1979. Solid line connecting dots is for temperature (°C), solid line connecting asterisks is for dew point (°C), dash-dotted line for 313 K isentrope, and dotted line showing moist adiabat for mean ABL parcel (or selected parcel if ABL not well-defined). Dew points colder than −40°C are plotted at −40°C.

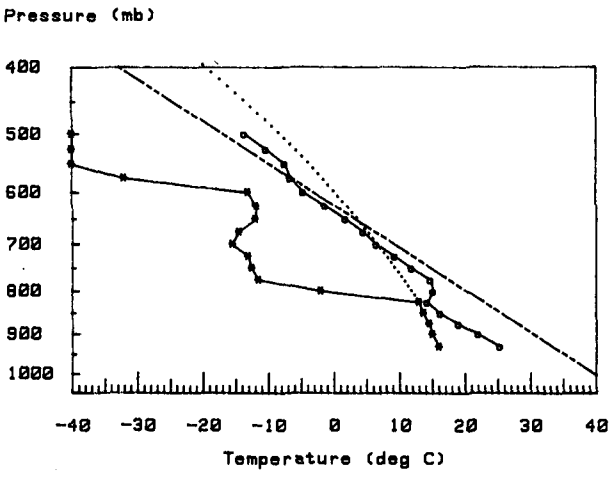

FIG. 6. As in Fig. 5 but for Dodge City, Kansas at 1715 GMT.

ature and moisture in the ABL have forms that can be described by scaled universal structure functions. Solutions for the mixed layer and surface layer are matched at their common boundary to obtain mixed layer formulations. The forms of the temperature and moisture structure functions come from Arya (1975).

The soil heat flux is parameterized after Bhumralkar (1975). The flux is assumed to be vertical, and the variation of surface soil temperature from an average value is presumed to be sinusoidal. Solving the heat conduction equation yields an expression for the soil heat flux. Evaluated at the surface,

$$GS = \left(\frac{wck}{2}\right)^{1/2} \times \left[\frac{1}{w}\frac{\partial TG}{\partial t} + TG - \text{TBAR}\right], \quad (5)$$

where

c volumetric heat capacity of the soil,
TG ground temperature,
TBAR 50 cm soil temperature (an acceptable average),
k thermal conductivity of the soil,
w frequency of oscillation ($=2\pi$ day^{-1}).

"Force-restore" methods after Bhumralkar (1975) and Deardorff (1977) provide the temperature and the mixing ratio at the ground. Solving the heat conduction equation for a layer between 50 and 1 cm below the ground surface gives the effective ground temperature

$$\frac{\partial TG}{\partial t} = \frac{(NR - SH - LH) - \left(\frac{wck}{2}\right)^{1/2}(TG - \text{TBAR})}{c + \left(\frac{ck}{2w}\right)^{1/2}}, \quad (6)$$

where w, c and k are as previously defined.

The soil moisture is found by assuming that surface soil moisture responds to three main processes: precipitation, evaporation and flux from below. The bulk soil moisture is assumed to be constant over the period. According to Deardorff (1977), the bulk soil moisture changes over a time scale of a few weeks, so it can be assumed constant for a 12 h period with little loss of accuracy. The surface soil moisture,

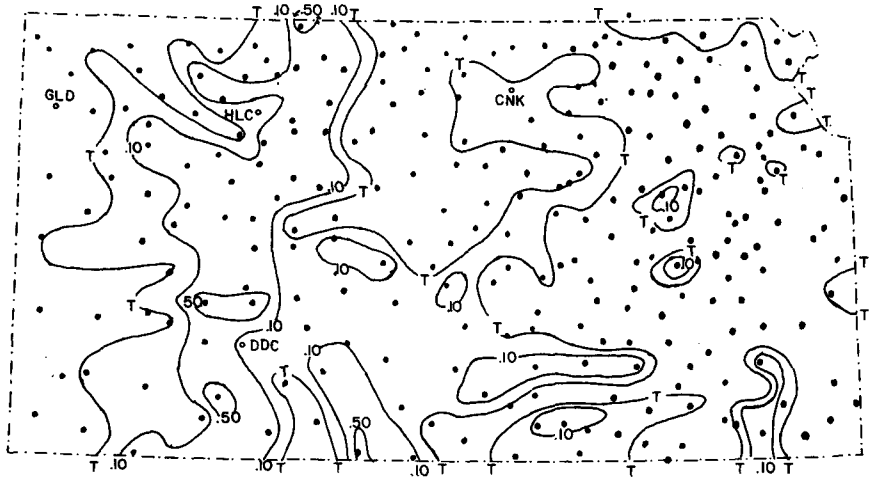

FIG. 7. Map of rainfall in Kansas on calendar day of 18April 1979. Contours are drawn for amounts as follows: trace (*T*), 0.10 and 0.50 inches. Dots indicate data points. Data from *Climatological Data for Kansas.*

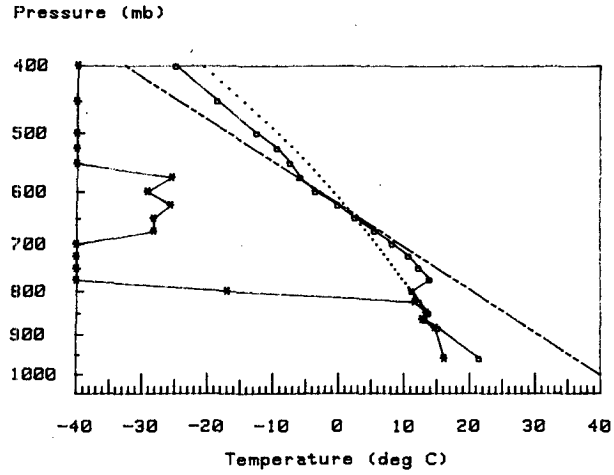

FIG. 8. As in Fig. 5 but for Concordia, Kansas at 2008 GMT.

which varies on a daily time scale, changes according to

$$\frac{\partial GW}{\partial t} = \frac{-c_1 LH}{\lambda \rho_\omega d_1 \mathrm{WMAX}} - c_2 \frac{(GW - \mathrm{GWB})}{\tau}, \quad (7)$$

where

GWB	% bulk soil saturation (top 50 cm),
GW	% surface soil saturation,
d_1	depth of diurnal cycle (=10 cm),
λ	latent heat of evaporation,
ρ_ω	density of H_2O = 1 g cc^{-1},
WMAX	field capacity soil moisture,
τ	period of cycle,
c_1, c_2	are nondimensional constants.

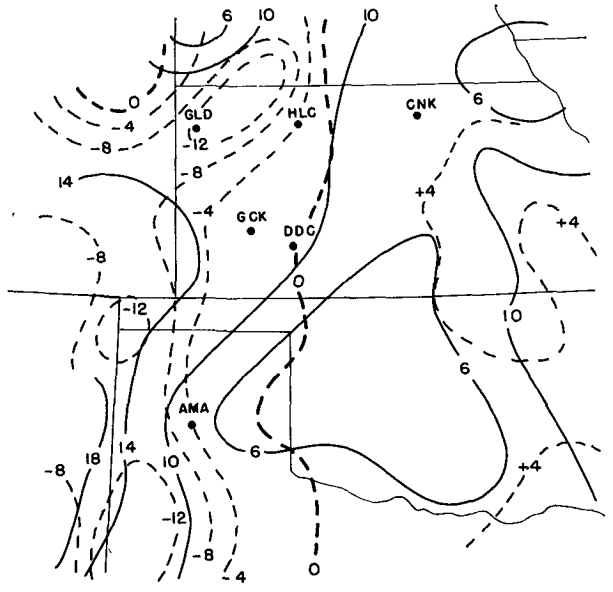

FIG. 9. Change in surface potential temperature and dew point between 1200 and 2200 GMT 19 April 1979. Solid lines for potential temperature (K) and dashed lines for dew point (°C).

TABLE 1. Temperature advection calculated at Dodge City, Kansas and Hill City, Kansas from surface analyses. Changes are for surface potential temperature in K. Time is GMT.

	DDC		HLC	
Time	Adv.	Obs.	Adv.	Obs.
12–13	0	0	<0.2	?
13–14	0	0.5	0	1.0
14–15	<0	2.4	0	2.4
15–16	<0	2.2	0.1	1.7
16–17	<0	2.9	0.4	2.4
17–18	<0	1.2	0.7	1.1
18–19	<0	1.2	0.5	1.2
19–20	<0	−0.6	0.4	1.7
20–21			0.2	0
Total	<0	9.8	2.3	11.5

Measurements taken over bare soil near Phoenix, Arizona in March from Jackson (1973) give values for c_1 and c_2. According to McCumber and Pielke (1981), details of soil mechanics (which depend on soil type) are not of major importance to the performance of this type of model.

The prediction of the depth of the boundary layer and strength of the inversion follows Zeman and Tennekes (1977). Their method assumes that the ABL depth changes result from turbulent entrainment of air above the inversion into the ABL. No allowance is made for the late afternoon transition to a nocturnal ABL since the convective outbreaks occurred prior to this time. The energy comes from the sensible heat flux at the surface, and the change of depth with time depends upon the strength of the inversion. Zeman and Tennekes use the turbulent kinetic energy budget to develop a simple set of equations to describe this process, i.e.,

$$\frac{\partial h}{\partial t} = \frac{-SH_h}{\Delta\Theta}, \quad (8)$$

where

h	the height of the top of the ABL,
$\Delta\Theta$	the strength of the inversion,
$-SH_h$	the sensible heat flux at the inversion,

and

$$\frac{\partial \Delta\Theta}{\partial t} = \gamma \frac{\partial h}{\partial t} - \frac{1}{h}(SH - SH_h), \quad (9)$$

where

γ	the lapse rate of potential temperature above the ABL,
SH	the sensible heat flux at the surface.

The ABL values of temperature and mixing ratio are found using the simple assumed structure in the ABL and a budget for the mixing ratio. The pressure level of the top of the inversion is known. The change in the height of the inversion has just been calculated so the amount of entrainment is known. This entrain-

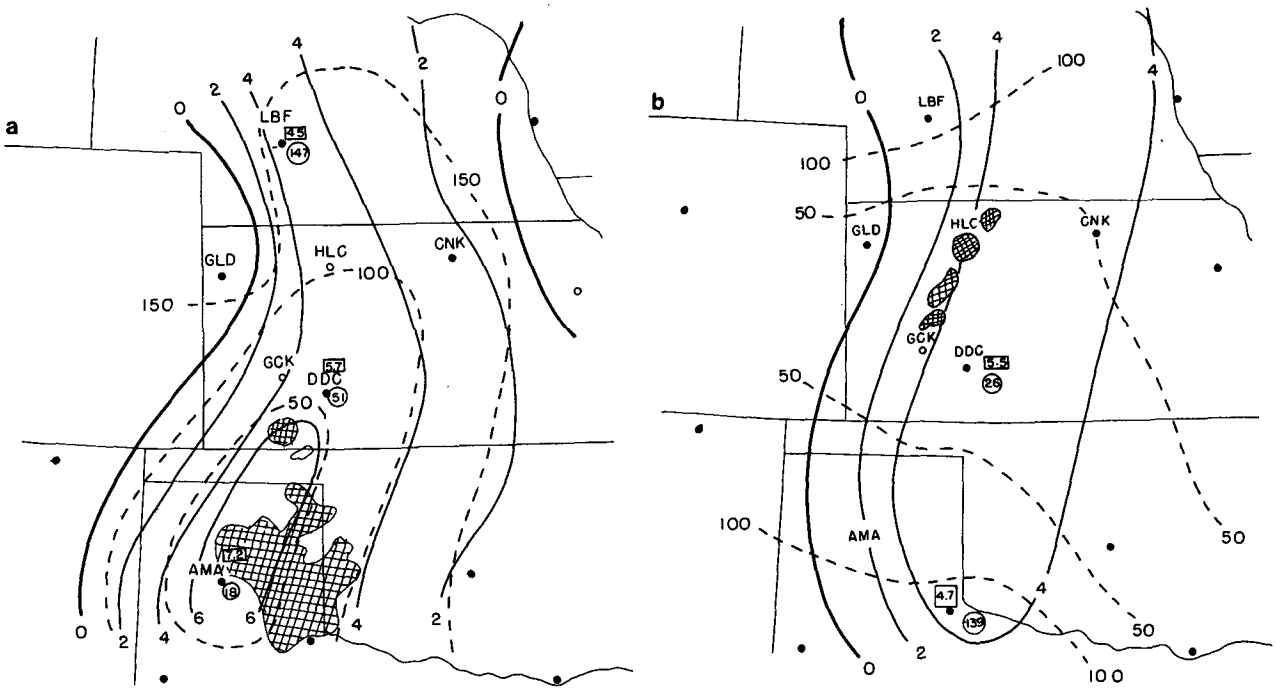

FIG. 10. Mesoscale analyses of potential convective energy (L) and convective inhibition (I) for (a) 1700 GMT and (b) 2000 GMT 19 April 1979. Solid lines are L (°C) and dashed lines are I (j kg^{-1}). Cross-hatching is for new radar echoes appearing between (a) 1800 and 2100 GMT and (b) 2100 and 2300 GMT. Numbers in boxes are point values of L, circled numbers for I. Dots denote data-point locations.

ment comes from the inversion layer so the new depth of the inversion can be found. Using the new values for the inversion strength, the potential temperature at the top of the inversion and the lapse rate of potential temperature in the inversion, the potential temperature of the ABL is calculated. This produces the new value of surface temperature. Figure 12 illustrates this process schematically.

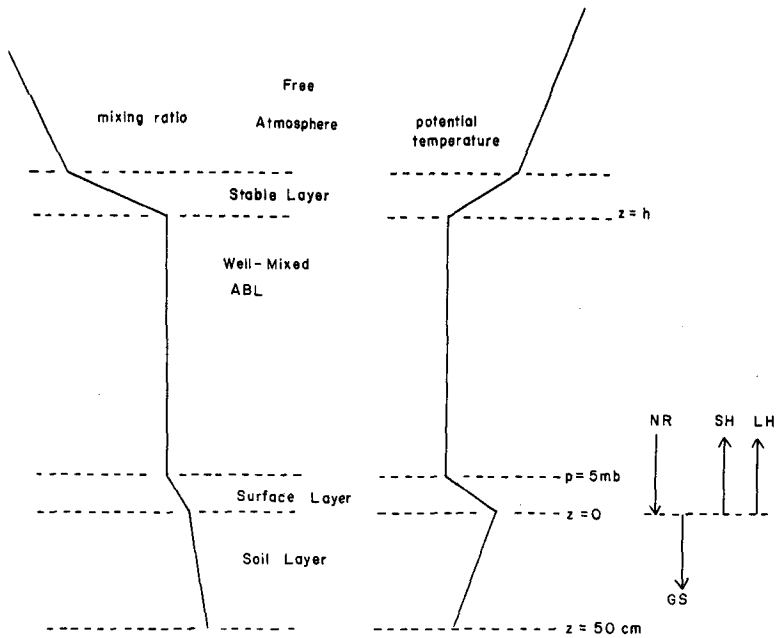

FIG. 11. Schematic diagram of model atmosphere showing hypothetical potential temperature and mixing ratio profiles and model layers. Also shown is flux diagram showing positive direction of fluxes at the surface.

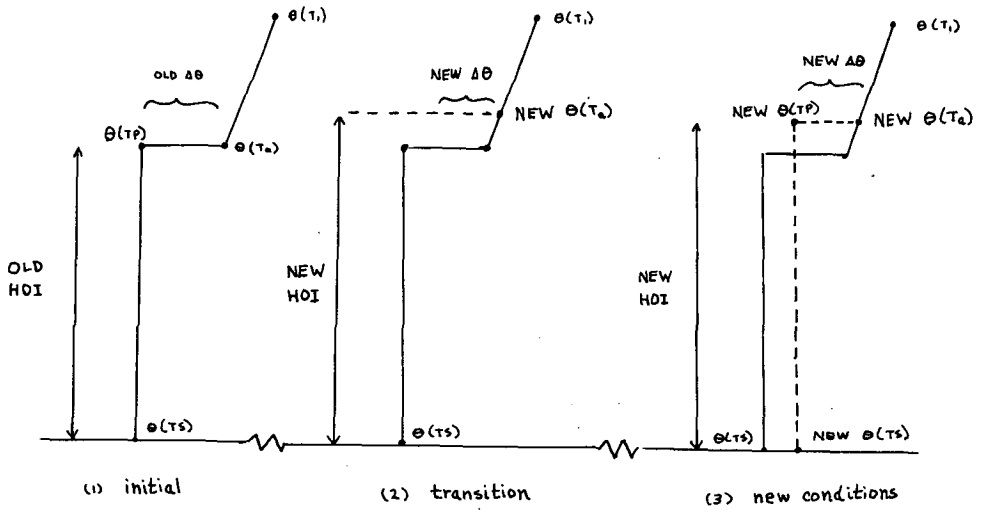

FIG. 12. Schematic diagram illustrating process of finding new ABL potential temperature from new inversion calculations. Horizontal axis is potential temperature.

Since no provision is made for a stable boundary layer in the model, reasonable operation of the model requires the initial sounding to have a specific form. In particular, a thin surface layer and a well-mixed ABL above are required. Realistically, the atmosphere is unlikely to possess either of these layers until after sunrise. Nevertheless, the initial sounding must be forced to conform immediately to the model requirements to prevent model collapse. Results from a study by Whiteman (1982) suggest that a small mixed layer appears within 15 min of ground illumination, so this unrealistic initialization is not drastic.

Data from the initial sounding between 400 mb and near the surface are used directly to initialize the model. The surface observation determines initial values of temperature and mixing ratio, and these values are set at the top of the surface layer, 5 mb above the ground. The ground temperature begins 0.1°C higher than the surface temperature, initially producing a positive sensible heat flux. The initial moisture for the ABL equals the surface value. The initial ABL depth including the surface layer is 90 m. The atmosphere above 90 m up to the first data point in the sounding is the first stable layer. The inversion strength for the first time step is derived by extending the first data point down to the 90 m level and calculating its potential temperature. Figure 13 shows this process. This operation creates an isothermal layer above the initial ABL, and the characteristics of this new layer determine the lapse rate in the stable layer.

This initialization procedure seems like a major modification to the sounding, but the actual changes are small enough to be barely detectable when plotted

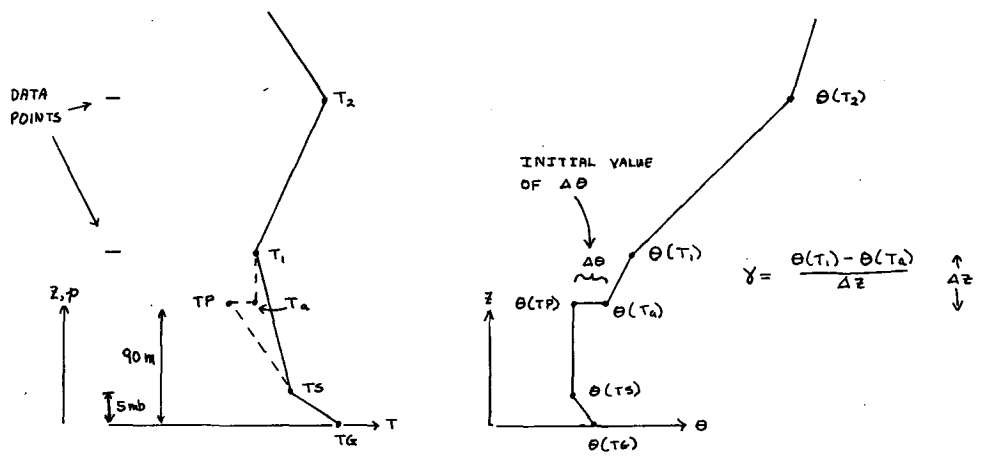

FIG. 13. Schematic diagram showing process of initialization of inversion from initial sounding. Vertical axis is height. Horizontal axis on left side is temperature, on right side, potential temperature.

on a pseudoadiabatic chart. For a typical sounding, the change in the dry static energy of the adjusted portion of the sounding is less than 0.1%.

5. Model results

Sensitivity tests performed with the model showed that soil moisture had the greatest effect on the partitioning of energy between sensible heat and latent heat fluxes. This, in turn, controlled the heating and growth of the ABL. Therefore, the soil surface moisture was treated carefully to ensure that the ABL moisture in the model did not deviate from surface observations.

To confirm the model's capability to simulate the ABL development, it was initialized with the observed 1100 GMT GLD sounding (Fig. 5a) and run until 2000 GMT. This initial sounding had a shallow moist layer near the ground capped by a strong inversion, with a large dry adiabatic layer aloft. By 2000 GMT (Fig. 5b) the observed GLD sounding had a huge, dry adiabatic, boundary layer without an inversion, due mostly to boundary layer heating and a modest amount of dry advection. When initialized with 20% soil surface wetness and 50% bulk soil wetness, the model produced the 2000 GMT sounding shown in Fig. 14. The model reproduced nearly all of the drying actually observed, and it duplicated quite accurately the very large ABL growth. The 4°C dewpoint difference between the model and the observations probably resulted from the dry advection at GLD.

None of the actual soundings were in the region where the convection occurred. The squall line developed between GLD and CNK, north of DDC. To investigate the ABL structure in the immediate region of the convective outbreak, the model was initialized with a hybrid sounding. The 1100 GMT analysis of surface conditions and both isentropic and isobaric analyses of upper air data aided in the construction of this sounding. Isobaric analyses were done at 500 and 700 mb. Most soundings from the eastern side of the network showed a deep, elevated, nearly adiabatic layer, with potential temperatures rising linearly from 311 to 313 K. Analyses for these two values of potential temperature yielded the top and bottom of this layer. Analyses were also done at 309, 305 and 301 K. Interpolation from the three nearest soundings (CNK, DDC and GLD) produced the data above 500 mb. Figure 15 shows this 1100 GMT hybrid sounding. The soil wetness parameters were set by using the past rainfall as a guide. The bulk soil wetness was set at 50%, similar to GLD and the initial surface soil wetness was set at 50% as well, since some rain fell during the previous day (see Fig. 7). Although less important, the rainfall pattern on 17 April closely resembled that of 18 April. The important aspect of this is the pattern, not the exact amounts, since no definite numerical relationship exists between rainfall and soil wetness. All that can be assumed with certainty is that more rainfall will lead to wetter soils.

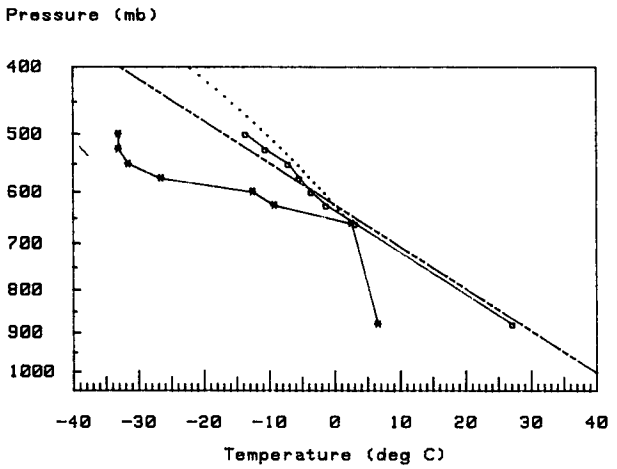

FIG. 14. As in Fig. 5 but for model output at 2000 GMT from GLD initial sounding.

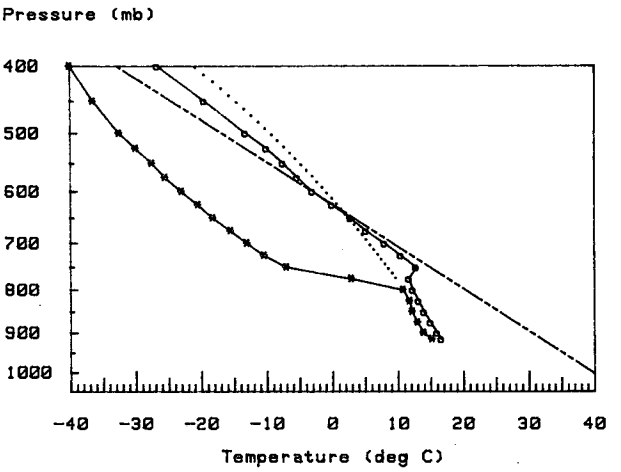

FIG. 15. As in Fig. 5 but for initial hybrid sounding, 1100 GMT.

The time variation of cloudiness was an important part of the model behavior. The initial clouds affected the energy budget of the ABL for the whole day only slightly, since the major portion of the heating took place during the middle of the day, after the clouds had dissipated. The presence of the clouds did slow the heating of the soil and, therefore, slowed the drying out of the soil as well. Thus, when the clouds dissipated later on, the soil was more moist during the period of greatest heating, which probably gave greater release of latent heat and less sensible heat than if the clouds had not been present. The values used for cloudiness appear in Table 2.

Changes aloft also affected the ABL development. Variations in the strength of the inversion affected the rate of growth of the ABL. Changes in moisture

TABLE 2. Clouds imposed in model run, expressed as percentages of complete cloud cover.

P (mb)	1100–1400 GMT	1400–1700 GMT
800	80	0
825	90	80
850	90	80
875	80	80
900	80	80

content of the air in the inversion affected the moisture budget in the boundary layer. The changes used in the model were derived from those observed at GLD. Subsidence between 1100 and 1400 GMT intensified the inversion above the ABL in the layer from 775 to 800 mb, increasing the temperature of this layer by more than 2°C. Between 1100 and 1700 GMT, cooling took place aloft, which enhanced ABL growth by reducing the stability above the ABL. The strongest cooling occurred between 650 and 750 mb, averaging slightly more than 2°C over the 6 h period. Table 3 details these changes.

The modeling results allowed the determination of the importance of various factors in the development of the lifted index and convective inhibition during the day. A comparison of the analyses at 1700 and 2000 GMT (see Fig. 10) clearly shows that inhibition dropped sharply in the convective region during these three hours. By varying the physical effects included in the model, conclusions could be drawn concerning the importance of each one to the changes in the potential convective energy and convective inhibition. Table 4 shows the results of the various runs.

The "plain" run (i.e., including surface heating, but with no clouds or imposed changes aloft) gave the most unstable values for lifted indices and nearly

TABLE 3. Changes imposed in model runs above the boundary layer, taken from Goodland, Kansas soundings. Levels not mentioned or times not covered had zero changes imposed.

	1100–1400 GMT		1400–1700 GMT	
P (mb)	T (°C)	Q (g kg^{-1})	T (°C)	Q (g kg^{-1})
500	−1.0	0	0	0
525	−0.6	0	0	0
550	−1.0	0	0	0
575	0	0	0	0
600	−0.6	−0.4	0	0
625	−1.0	+0.4	0	0
650	−1.2	+0.4	−0.9	0
675	−1.2	0	−1.0	0
700	−1.2	0	−1.0	0
725	−0.8	0	−1.2	0
750	−0.6	−0.4	−1.0	0
775	+3.0	−3.6	0	0
800	+2.0	−8.0	0	0

TABLE 4. 2100 GMT model results using initial hybrid sounding with physics included as indicated. *PH* is pressure level of inversion (mb), *TS* is temperature at bottom of ABL (°C), *QS* is mixing ratio of ABL (g kg^{-1}), *L* is potential convective energy (°C) and *I* is convective inhibition (j kg^{-1}). All runs include surface heating.

Physics	*PH*	*TS*	*QS*	*L*	*I*
Plain	759	25.0	10.9	6.0	27.4
+ clouds	768	24.1	11.0	5.7	34.7
Imposed changes (no clouds)	772	25.4	10.0	5.1	13.5
All	780	24.6	10.4	5.2	16.1

the highest amounts of inhibition. Adding morning clouds to the run produced a shallower, cooler and more moist ABL. The clouds reduced the heating, allowing less ABL growth than in the plain case, and keeping it cooler. The lifted index dropped slightly and the inhibition increased by 25%.

Imposing the changes aloft without clouds but including the basic heating of the boundary layer gave a warmer and drier ABL, with less instability and lower amounts of inhibition. Without the heating, the changes aloft only slightly affected the convective inhibition. The lowering of the inversion by itself increased the inhibition from 113 to 200 j kg^{-1}, while the cooling aloft, by itself, reduced the inhibition from 113 to 47 j kg^{-1}. Notice that the ABL for this run was actually shallower than that for either the plain or the cloudy run. The imposed changes increased the stability above the ABL enough to retard the growth of the ABL throughout the period and produced the shallower ABL. Unlike the run with clouds, the solar heating in this run equaled that in the plain run, so the temperature in the ABL rose higher than for either of the other runs. Although the ABL entrained less air from above, thus remaining shallower, the entrained air was drier. This was sufficient to produce a lower ABL mixing ratio for this run.

The inclusion of all of the factors resulted in the sounding shown in Fig. 16. The lifted index was substantial (5.2) and the convective inhibition was smaller than any observed (16.1). This inhibition was 40% lower than the nearest observation of 26 j kg^{-1} at DDC. Inhibition of this magnitude requires a parcel vertical velocity of ~5.7 m s^{-1}, higher than that typically found in a convective ABL. The convective echoes were detected 15–30 min after 2100 GMT. Simple extrapolation of ABL growth shows that the inversion would have just been fully eroded by 2130 GMT.

6. Conclusions

The combination of results from observational analysis and modeling shows that the convection in

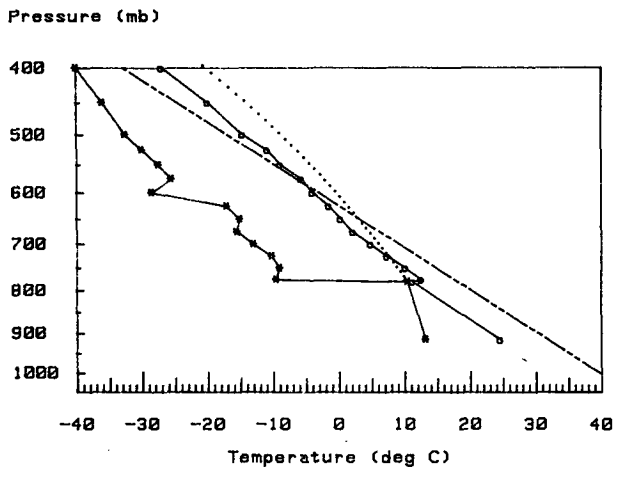

FIG. 16. As in Fig. 5 but for 2100 GMT model output from hybrid initial sounding.

western Kansas on 19 April 1979 began in a region of substantial potential convective energy and minimum convective inhibition. Strong boundary layer heating in the presence of moderate soil moisture and early morning cloudiness reduced the convective inhibition during the day. Thicker clouds caused a sharp reduction in the heating in eastern Kansas (at CNK for example). With very dry soils, the ABL grew quickly in extreme western Kansas, and convection inhibition dropped sharply. This resulted in a lack of sufficient moisture for potential convective energy to be significant (such as at GLD).

The heating and moistening of the ABL were balanced in a band running between HLC and DDC in western Kansas. The weak convergence associated with the differential heating, oriented in a similar, linear fashion, further contributed to destabilization. Cooling aloft enhanced destabilization, but subsidence at the inversion stabilized the atmosphere, nearly canceling the effects of cooling aloft. The convection started when the convective inhibition in this region dropped enough to allow ABL turbulence, combined with the weak vertical motion due to convergence, to lift ABL parcels to their level of free convection. This behavior was found in other cases of convection in this part of the country. Colby (1980) showed that a squall line in Oklahoma broke out when negative buoyancy in a sounding became negligible. The analysis of two other SESAME cases (not discussed here) also showed that low convective inhibition is an important predictor for convective outbreaks. In addition, Carlson *et al.* (1980) showed that their Lid Strength index, which includes a measure of the strength of the capping inversion, was a maximum in the region of convective outbreak during AVE-SESAME I, 10 April 1979. Finally, Foote and Wade (1982) noted that prior to a Colorado hailstorm, the "negative energy" in a prestorm sounding was small.

The prediction of the diurnal change of convective inhibition and convective energy would enable the precise forecasting of convective outbreaks. The potential for simple modeling of these quantities is currently being tested and may prove feasible for limited regions.

Acknowledgments. This paper came from the author's Ph.D. thesis written under the guidance of Professor F. Sanders at Massachusetts Institute of Technology. The author wrote the manuscript as an Air Force Geophysics Scholar at AFGL/LYT, Hanscom AFB, MA. All of the support is gratefully acknowledged. I also thank the reviewers for contributing excellent and constructive criticism. This research was supported by the National Science Foundation under Grant No. ATM 80-19301.

REFERENCES

Arya, S. P. S., 1975: Geostrophic drag and heat transfer relations for the atmospheric boundary layer. *Quart. J. Roy. Meteor. Soc.*, **101**, 147–161.

Beebe, R. G., 1958: Tornado proximity soundings. *Bull. Amer. Meteor. Soc.*, **39**, 195–201.

Bhumralkar, C. M., 1975: Numerical experiments on the computation of ground surface temperature in an atmospheric general circulation model. *J. Appl. Meteor.*, **14**, 1246–1258.

Carlson, T. N., R. A. Anthes, M. Schwartz, S. G. Benjamin and D. G. Baldwin, 1980: Analysis and prediction of severe storms environment. *Bull. Amer. Meteor. Soc.*, **61**, 1018–1032.

Colby, F. P., Jr., 1980: The role of convective instability in an Oklahoma squall line. *J. Atmos. Sci.*, **37**, 2113–2119.

Cooper, H. J., M. Garstang and J. Simpson, 1982: The diurnal interaction between convection and peninsula-scale forcing over south Florida. *Mon. Wea. Rev.*, **110**, 486–503.

Darkow, G. L., P. M. Kuhn and V. G. Suomi, 1958: Surface thermal patterns as a tornado forecast aid. *Bull. Amer. Meteor. Soc.*, **39**, 532–537.

Deardorff, J. W., 1977: A parameterization of ground surface moisture content for use in atmospheric prediction models. *J. Appl. Meteor.*, **16**, 1182–1185.

Foote, G. B., and C. G. Wade, 1982: Case study of a hailstorm in Colorado. Part I: Radar echo structure and evolution. *J. Atmos. Sci.*, **39**, 2828–2846.

Galway, J. G., 1956: The lifted index as a predictor of latent instability. *Bull. Amer. Meteor. Soc.*, **34**, 528–529.

Holle, R. L., and M. W. Maier, 1980: Tornado formation from downdraft interaction in the FACE mesonetwork. *Mon. Wea. Rev.*, **108**, 1010–1028.

Jackson, R. D., 1973: Diurnal changes in soil water content during drying. *SSSA Special Publication*, No. 5, Soil Science Society of America, Madison, 37–55.

Katayama, A., 1972: A simplified scheme for computing radiative transfer in the troposphere. Tech. Rep. No. 6, Dept. of Meteorology, University of California, Los Angeles, 77 pages.

Maddox, R. A., L. R. Hoxit and C. F. Chappell, 1980: A study of tornadic thunderstorms interacting with thermal boundaries. *Mon. Wea. Rev.*, **108**, 322–336.

Mahrt, L., 1976: Mixed layer moisture structure. *Mon. Wea. Rev.*, **104**, 1403–1407.

Matthews, D. A., 1981: Observations of a cloud arc triggered by thunderstorm outflow. *Mon. Wea. Rev.*, **109,** 2140–2157.

McCumber, M. C., and R. A. Pielke, 1981: Simulation of the effects of surface fluxes of heat and moisture in a mesoscale numerical model. 1. Soil layer. *J. Geophys. Res.*, **86,** 9929–9938.

Miller, D. A., and F. Sanders, 1980: Mesoscale conditions of the severe convection of 3 April 1974 in the east-central United States. *J. Atmos. Sci.*, **37,** 1041–1055.

Petterssen, S., 1956: *Weather Analysis and Forecasting. Vol. II: Weather and Weather Systems.* McGraw-Hill, p. 135.

Sanders, F., and R. J. Paine, 1975: The structure and thermodynamics of an intense mesoscale convective storm in Oklahoma. *J. Atmos. Sci.*, **32,** 1563–1579.

Schaefer, J. T., 1976: Moisture features of the convective boundary layer in Oklahoma. *Quart. J. Roy. Meteor. Soc.*, **102,** 447–451.

Showalter, A. K., 1953: A stability index for thunderstorm forecasting. *Bull. Amer. Meteor. Soc.*, **34,** 250–252.

Sun, W.-Y., and Y. Ogura, 1979: Boundary-layer forcing as a possible trigger to a squall-line formation. *J. Atmos. Sci.*, **36,** 235–254.

Uccellini, L. W., 1975: A case study of apparent gravity wave initiation of severe convective storms. *Mon. Wea. Rev.*, **103,** 497–513.

——, and D. R. Johnson, 1979: The coupling of upper and lower tropospheric jet streaks and implications for the development of severe convective storms. *Mon. Wea. Rev.*, **107,** 682–703.

Whiteman, C. D., 1982: Breakup of temperature inversions in deep mountain valleys: Part I. Observations. *J. Appl. Meteor.*, **21,** 270–289.

Zeman, O., and H. Tennekes, 1977: Parameterization of the turbulent energy budget at the top of the daytime atmospheric boundary layer. *J. Atmos. Sci.*, **34,** 111–123.